Contents

1 Purpose of the dissertation

As will be discussed in the following section interfaces have a crucial impact on the properties of materials. As the size of material systems decreases to nanoscale properties of materials are greatly influenced by interfaces. Interface thermodynamics of fluid systems was developed by Gibbs [1]. Considering interfaces when one of the coexisting phases is solid Gibbs pointed out to some fundamental differences between fluids and solids. While thermodynamics of planar fluid-fluid interfaces is well developed, treatment of solid-fluid and solid-solid interfaces is not.

In this dissertation we will develop a thermodynamic treatment for solid-fluid interfaces, solid grain and phase boundaries. The treatment will provide expressions for interface free energy, adsorption equation, Maxwell type equations and Gibbs-Helmholtz type equations for thermodynamic integration.

The developed theory will be applied in computer simulations. In this study we will design techniques of computations and compute excess interface properties for systems mentioned above. We will also test the correctness of the theory by comparing predictions with behavior of interface properties computed directly from atomistic simulations.

In this proposal I first give a brief introduction with examples of physical processes in which interfaces play a crucial role. Then I outline the problems that will be addressed in this work and describe our approach. In the following sections I present current results and discuss ongoing work.

2 Introduction

Interfaces play a crucial role in material science [2]. Materials are generally not single crystals but made of grains with different crystallographic orientations separated by interfaces. The sizes of grains range from nanoscale to microscale. Orientation, shape and size of grains and interfaces represent a microstructure of a material. Because properties of interfaces are different from properties of bulk material microstructure (grain size, interfaces) determines mechanical, thermal and electronic properties of materials.

For the reasons above it is important for technological applications to understand thermodynamic properties that determine microstructure. During a process of solidification, nuclei of solid phase appear in the melt. The rate of nucleation will determine the average grain size of material. This rate depends on solid-liquid interface free energy, which is a reversible work of creation of a solid-liquid interface. As a solid nucleus grows solidification happens faster along some directions resulting in dendritic growth. Snowflakes are more familiar example of dendrites (nucleation and growth of ice in vapor). The process of dentritic growth is determined by anisotropy of interface free energy [3].

Nucleus of unstable phase can nucleate if solid-liquid interface free energy of this phase is lower then the interface free energy between melt and stable phase [4]. For

example, nucleation of metastable bcc phase instead of stable fcc occurs in Fe and Ni based alloys when melt is rapidly quenched [5, 6, 7, 4]. From these examples we conclude that both magnitude and anisotropy of γ determine microstructure of materials, which in turn determines the properties of materials [3].

In multicomponent systems with interfaces some components tend to have higher concentration in the interface region. This phenomenon is called interface segregation [2] and it is governed by the "desire" of the system to minimize its interface free energy. Different chemical composition in the interface region can be either beneficial or catastrofic for the properties of materials. Grain boundaries (GB) are preferable sites of segregation of impurities. GB segregation can cause brittle failure of materials, environmentally assisted fatigue and corrosion.

Interfaces and GBs are preferable routes for electromigration in microelectronic devices [8]. While momentum transfer from the electric current to atoms is negligible in the bulk material, atoms in the boundaries are able to diffuse in the direction of the current. This process shortens the lifetime of microelectronic devices.

The magnitude of γ determines contact angles in wetting process. By manipulating thermodynamic variables, one can modify interface free energies and in turn change contact angles. This phenomenon is employed in electrowetteng [9], where one can manipulate with interface free energies in the system containing droplet on the substrate by varying external electric field. The ability to achieve desired contact angles found applications in digital microfluidcs (lab-on chip technology) [10]. Using electrowetting large droplet can be split into smaller droplets of the desired size. These discrete droplets are then used to store and transport chemical substances and to cause chemical reactions by merging the individual droplets together. This ability to perform complex operations step by step (by adding droplets in a discrete way) is useful in applications such as chemical synthesis and biological assay.

The several examples mentioned above demonstrate that interface phenomena plays a crucial role in many physical processes.

3 Goal and approach

Thermodynamics of interfaces was developed by Gibbs [1]. He described a system of two phases in equilibrium separated by inhomogeneous interface region by introducing the concept of a dividing surface. The real system was represented as two homogeneous bulk systems and a dividing surface with the properties of the bulk regions extrapolated all the way to the dividing surface. Gibbs derived an expression for interface free energy γ as a reversible work of creation of unit of interface in terms of excesses of thermodynamic properties computed for a given position of the dividing surface. He also derived an adsorption equation that gives a variation of γ in terms of intensive properties that describe equilibrium between phases. Discussing solid-liquid interfaces Gibbs pointed out that interfacial area can be increased by elastic stretching of the interface. This later work is done by interface stress. Deriving the adsorption equation

for such interfaces he considered variations at constant area.

The adsorption equation for fluid systems was generalized by Cahn [11]. He used the Gibbs expression of γ derived using the notion of dividing surface to derive an adsorption equation that contains term with excess volume of interface. Cahn's formulation pointed out very important details of interface thermodynamics. The adsorption equation predicts the number of degrees of freedom of the system. He demonstrated how constraints of bulk equilibrium modify adsorption equation and affect the choice and number of appropriate independent variables. Cahn also analyzed Maxwell relations implied by the adsorption equation.

As was pointed out by Gibbs, if one of the phases is solid then the thermodynamic state of a system can vary by elastic deformation. The adsorption equation that includes elastic work was derived for a single component surface by Shuttleworth [12]. He denoted a partial derivative of γA with respect to strain per unit area as interface stress τ and pointed out to its tensor nature. However, expression for τ as an excess quantity was not derived.

In the case of solid-fluid interfaces in multicomponent systems, an expression for γ cannot be derived using dividing surface unless the solid is hydrostatic. A different approach has to be developed to derive interface free energy as a work of creation of unit of interface.

Thermodynamic treatment of solid-solid interfaces is even more challenging, because they support shear stresses parallel to the interface. The effect of lateral and shear stresses on interface free energy in solid-solid two phase systems is not present in the current thermodynamic treatments.

The goal of this work is to address all the theoretical difficulties mentioned above. We will derive an expression for γ for interfaces in one and two phase multicomponent systems with both substitutional and interstitial components. We will incorporate effects of lateral deformation and derive expression for interface stress for solid-fluid and solid-solid interfaces. In case of solid-solid interfaces we will include effects of shear stresses parallel to the interface.

To develop interface thermodynamics we will use the thermodynamic description of solids developed by Larche and Cahn [13, 14]. They derived equilibrium conditions between two solid phases separated by a coherent or incoherent interface. These equilibrium conditions are essential for derivation of γ and adsorption equation.

After the thermodynamic treatment is developed we will apply it to the study of metallic systems in computer simulations. It is important to note that the theory is general and not specific to any particular type of interactions. It can be applied to ceramics or polymers as well. To study interface properties we will employ atomistic simulations with interactions between atoms described by embedded atom method (EAM) [15] potentials. These semi-empirical potentials provide more realistic description of properties of materials than pair potentials. To model the motion of atoms we will use molecular dynamics (MD) and Monte Carlo (MC) methods in various ensembles. Atomistic simulations allow for the study of interface phenomena on a very detailed level. Quantities required for thermodynamic treatment like energies, diffusion potentials and others

are very difficult or even impossible to measure directly in experiment, but are readily available in computer simulations.

4 Results obtained so far

4.1 Solid Surface

The surface free energy γ and the surface stress τ_{ij} are fundamental quantities in surface thermodynamics. Gibbs [1] defined the surface free energy as reversible work per unit area needed to create a new surface, and the surface stress as reversible work of elastically stretching the surface. These two quantities are related by [12]

$$\tau_{ij} = \delta_{ij}\gamma + \frac{\partial \gamma}{\partial e_{ij}}, \quad i,j = 1,2, \tag{1}$$

where the derivative is taken at a constant temperature, e_{ij} is a strain tensor of the surface and δ_{ij} is the Kronecker symbol. While γ is a scalar, the surface stress $\hat{\tau}$ is a symmetrical second rank tensor. These quantities are usually of the same order of magnitude. Due to the second term in Eq. (1), components of $\hat{\tau}$ can be larger than γ, smaller, or even negative.

In contrast to solids, γ and τ of liquids are numerically equal because liquids respond to strains by exposing more or less atoms to the surface without changing γ, resulting in $\partial\gamma/\partial e_{ij} = 0$ [16]. At high temperatures, γ of a solid can exceed the sum of the liquid-vacuum and solid-liquid free energies. To minimize the free energy, the solid surface can premelt, creating a thin liquid-like layer [17]. Gurney [18] argued that because at high temperatures surface atoms can migrate like in a liquid, the surface free energy should become equal to the surface stress. This assumption was later used in the experimental work of Bailey and Watkins [19]. Herring [20] disagreed with Gurney's conclusion, questioning the way Gurney related the chemical potentials of the surface atoms to the surface stress.

Unfortunately, most of the data for surface stresses reported in the literature refer to $0\,K$ or a certain fixed temperature, making it difficult to determine whether τ and γ converge with temperature. The temperature dependence of γ was studied experimentally [21] and by atomistic simulations [22, 23], and it was found that γ decreases with temperature. The experiments of Vermaak and Wilsdorf [21] indicated that the second term in Eq. (1) linearly increased with temperature.

Eq. (1) can also be applied to solid-liquid interfaces, provided the derivative is taken along a constant-temperature direction on the solid-liquid coexistence surface in the parameter space. It can be expected that τ and γ would be again different, but this has not been tested experimentally. Recent atomistic simulations indicate that τ of solid-liquid interfaces can be positive or negative, depending on the material [24].

The goal of this work is to clarify the behavior of the surface stress and surface free energy with temperature, particularly near the bulk melting point. We employed

atomistic computer simulations using a (110) copper surface as a model. For the interpretation of the surface premelting behavior, we have also studied isolated solid-liquid and liquid-vacuum interfaces.

Consider an elemental solid in a non-hydrostatic state of strain whose plane surface is exposed to vacuum. A reversible work required to create a surface is equal to difference of Helmholtz free energies of the system on N atoms that has surface and the bulk system of N atoms [25]

$$\gamma A = F - F^s \tag{2}$$

where A is the surface area, γ is the specific surface free energy. Differentiating Eq. (2) we derive an adsorption equation which gives reversible variation of the total excess free energy [25]

$$d(\gamma A) = -[S]_X \, dT - [N]_X \, df^s + \sum_{i,j=1,2} [\sigma_{ij} V]_X \, de_{ij}, \tag{3}$$

where the state variables are temperature T, the Helmholtz free energy per atom of the bulk solid f^s, and the elastic strain tensor $\hat{e}$. The expressions in the square brackets are computed by [11]

$$[Y]_X \equiv \frac{\begin{vmatrix} Y & X \\ Y^s & X^s \end{vmatrix}}{X^s} = Y - Y^s X / X^s \tag{4}$$

where X and Y are any two of the extensive quantities S, N or $\sigma_{ij}V$. The superscript s refers to properties of a homogeneous solid region chosen as a comparison system. $[Y]_X$ has a meaning of a total excess of quantity Y when the system with a surface has the same amount of property X as the bulk homogeneous system. Since $[X/X] = 0$, one of the terms in Eq. (3) is necessarily zero, reflecting the constraint imposed by the bulk equation of state. If $X = N$ Eq. (3) becomes

$$d(\gamma A) = -[S]_N \, dT + \sum_{i,j=1,2} [\sigma_{ij} V]_N \, de_{ij}, \tag{5}$$

The last term in Eq. (5) corresponds to the work of elastic stretching of the surface. Partial derivative of γA with respect to strain per unit area defines surface stress tensor whose components can be computed from the determinants

$$\tau_{ij} = \frac{1}{A} \frac{\partial(\gamma A)}{\partial e_{ij}} = \frac{[\sigma_{ij} V / N]}{A} = \frac{\begin{vmatrix} \sigma_{ij} V & N \\ \sigma^s_{ij} V^s & N^s \end{vmatrix}}{A N^s} = \frac{\sigma_{ij} V - \sigma^s_{ij} V^s N / N^s}{A} \tag{6}$$

By integrating the adsorption equation (Eq. 5), one could compute value of γ along some trajectory as a function of temperature and elastic strains. However, in applications excess entropy is rarely accessible. To bypass the problem of computing $[S]_N$ we

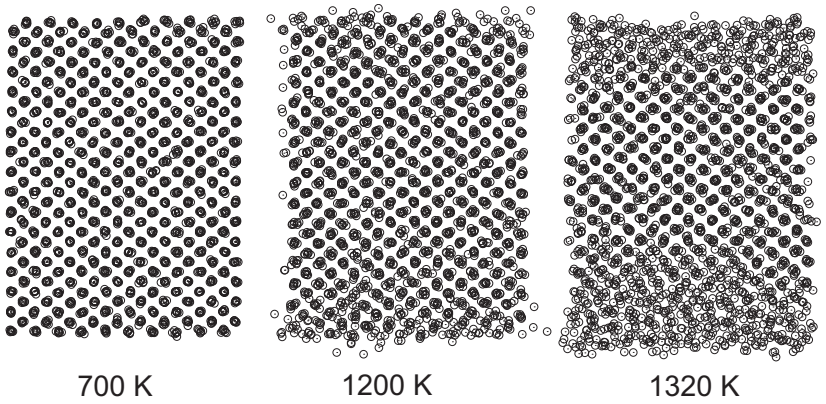

Figure 1: Typical MC snapshot of the solid film at three temperatures. Atomic positions are projected on the $(1\bar{1}0)$ plane parallel to the page. The surface structure is perfectly ordered at low temperatures and premelted at high temperatures.

combine Eq. (2) and Eq. (5) to derive a Gibbs-Helmholtz type equation suitable for thermodynamic integration

$$d\left(\frac{\gamma A}{T}\right) = -\frac{[U]_N}{T^2}dT + \frac{1}{T}\sum_{i,j=1,2}\tau_{ij}Ade_{ij}. \tag{7}$$

where $[U]_N$ is the excess energy. All the properties in Eq. (7) are readily accessible in computer simulations.

Using Eq. (6) and Eq. (7) we computed the surface stress and surface free energy of (110) copper surface as a function of temperature. In our simulations we used copper as a model material with interactions in copper described by EAM potential [26]. The potential accurately reproduces cohesive energy, elastic constants, thermal expansion and formation energies of defects. The melting point predicted by this potential $T_m = 1327K$ is in a very good agreement with the experimental value ($T_{exp} = 1356K$).

To model the copper surface at finite temperatures we used Monte-Carlo (MC) simulations in NVT ensemble. In the MC simulations, the system volume and temperature are fixed while the atoms can move. At each MC step, a randomly chosen atom is displaced by a random amount in a random direction and this move is accepted or rejected by the Metropolis algorithm. At each temperature, the initial configuration was brought to equilibrium by 10^5 MC steps per atom, followed by a production run of 6×10^5 additional MC steps. Snapshot files containing instantaneous atomic positions were saved every 30 MC steps and used in subsequent calculations of stresses, energies and other properties.

The solid surface calculations were performed at temperatures from 0 to $1320K$, the liquid surface calculations at 1300, 1327 and $1350K$, and the solid-liquid interface calculation at $1327K$ only.

Figure 1 demonstrates snapshots of the simulated system at different temperatures.

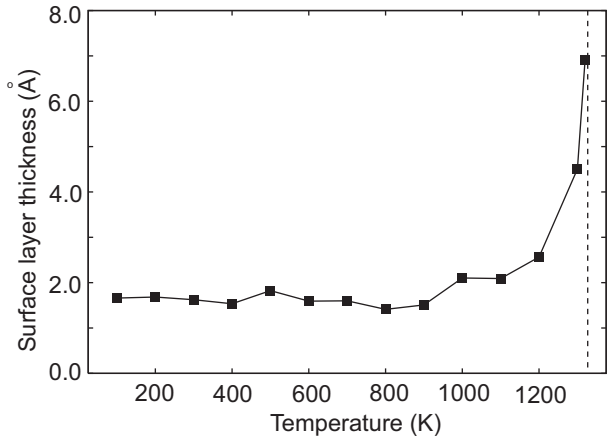

Figure 2: Thickness of the premelted surface layer as a function of temperature. The vertical dashed line indicates the bulk melting point.

As the temperature increases and approaches the melting point the solid surface premelts. In the immediate vicinity of the melting point the surface is covered by 7 Å thick layer of liquid. The thickness of the melted layer as a function of temperature is illustrated in Figure 2. Since the surface is almost liquid one could expect that γ and τ would converge and become identical as for liquid.

Figure 3 demonstrates behavior of γ and τ as a function of temperature. γ for the liquid surface was computed separately. Although the solid surface is covered with a relatively thick (e.g., about 7 $\mathring{A}$ at $1320K$) liquid-like film at temperatures approaching T_m, the free energy of the premelted surface remains quite different from the free energy of the liquid-vacuum interface or from the surface stress. This difference can be attributed to the excess quantities associated with the interface between the premelted layer and the bulk solid. Neglecting interactions ("disjoining potential") between these interfaces, the following relations should hold near T_m:

$$\gamma = \gamma^{sl} + \gamma^{l}, \tag{8}$$

$$\tau = \tau^{sl} + \gamma^{l}. \tag{9}$$

where γ^{sl} is solid-liquid interface free energy, τ^{sl} is solid-liquid interface stress and γ^{l} is surface free energy of liquid. In these relations, $\gamma = 1.130$ J/m^2, $\gamma^{l} = 0.925 \pm 0.018$ J/m^2 and $\tau = 0.83 \pm 0.012$ J/m^2 have been determined from the MC simulations. Solving these equations for γ^{sl} and τ^{sl}, we obtain $\gamma^{sl} = 0.199 \pm 0.018$ J/m^2 and $\tau^{sl} = -0.088 \pm 0.018$ J/m^2. The solid-liquid interface free energy compares well with the experimental value $\gamma^{sl} = 0.177$ J/m^2 from indirect measurements for an average orientation [27]. We computed τ^{sl} performing a simulation of solid-liquid coexistence at melting point. The computed value $\tau^{sl} = -0.11 J/m^2$ is also negative and in a close agreement with the estimate from surface simulations (Eq. (9)).

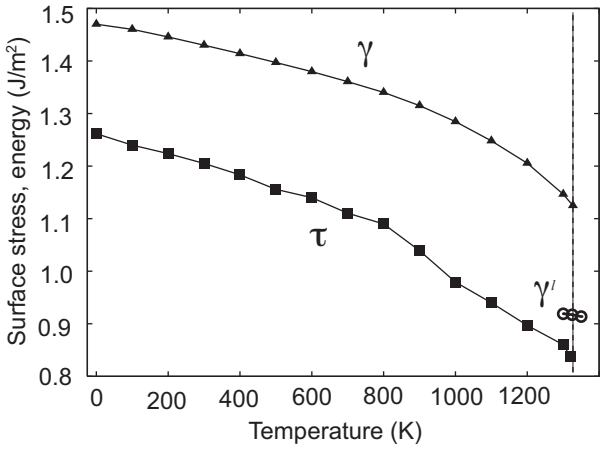

Figure 3: Temperature dependence of the excess free energy and stress of the (110) surface. Three values of the free energy, γ^l, of the liquid-vacuum interface are shown for comparison. The vertical dashed line indicates the bulk melting point.

4.2 Binary-solid liquid interface

The interface free energy γ is one of the most fundamental quantities in interface thermodynamics. For fluid systems the Gibbs adsorption equation expresses the differential of γ through differentials of intensive variables. The differential coefficients of the adsorption equation are excess quantities introduced by Gibbs using the concept of a dividing surface. Discussing solid-liquid interfaces, Gibbs treated the solid as a single-component substance and placed the dividing surface so that the interface excess of this component would vanish. This resulted in the adsorption equation that did not contain a term with the chemical potential of the solid component. As was recently pointed out [28], this procedure cannot be easily extended to binary or multicomponent solids. No choice of the dividing surface can guarantee that the excesses of all solid components would vanish simultaneously.

The complication with a proper definition of γ for multicomponent systems arises from two sources. One is that the state of stress of a solid can be non-hydrostatic. As was shown by Gibbs, a non-hydrostatically stressed solid can be equilibrated with three liquids having different chemical potentials of the components forming the solid. This means that chemical potentials of such components inside the solid are *undefined*. This was exactly the reason Gibbs chose to eliminate the interface excess of the solid component. Secondly, the Gibbsian construction of the dividing surface is just one possible way of introducing excess quantities. Cahn [11] proposed a more general formulation of the adsorption equation, in which the differential coefficients are defined without using the concept of a dividing surface. Instead, they are expressed via certain determinants composed of extensive properties of the system, as will be discussed below. Taking volume as one of such properties is equivalent to introducing a dividing surface, but this is only one particular case in Cahn's formulation [11].

Cahn's [11] adsorption equation was derived for interfaces between fluids and hydrostatically stressed solids. Solid-liquid coexistence in multicomponent non-hydrostatic systems was extensively analyzed by Larche and Cahn [13, 14]. They showed that under equilibrium conditions, the chemical potentials of all interstitial components in the solid exist and are equal to their chemical potentials in the liquid. For substitutional components the diffusion potential $M_{\alpha\beta}$ is constant everywhere in the system and equal to the difference between the chemical potentials of components α and β in the liquid [13, 14]. Larche and Cahn analyzed equilibrium between bulk phases and did not address interface thermodynamics.

In our previous work [25] we proposed an extension of Cahn's adsorption equation [11] to the non-hydrostatic case of a planar solid-fluid interface in a single-component system. More recently we have generalized this formalism by extending it to binary systems. We used the Larche-Cahn [13, 14] equilibrium conditions as the starting point in order to express the interface free energy γ and interface stress as excesses of appropriate thermodynamic potentials. We also derived a generalized adsorption equation and a Gibbs-Helmholtz-type differential equation that can be conveniently applied for thermodynamic integration in atomistic computer simulations.

In recent years, thermodynamic properties of interfaces have been studied by different simulation methods [29, 24, 30, 31, 32]. The interface free energy was computed by the cleavage technique [33, 34], the capillary fluctuation method (CFM) [35], and thermodynamic integration [23, 22, 25]. Unfortunately, the cleavage technique can be only applied to single-component systems or to binary systems where the solute component is insoluble in one of the phases. The CFM method was employed for calculations of γ in hard-sphere [36] and Lennard-Jones systems [37, 24, 38]. Thermodynamic integration was successfully applied to surfaces [23, 22, 25] but not to interfaces in binary two-phase systems. This work appears to be the first one where γ was computed by thermodynamic integration along a solid-liquid coexistence path.

To derive an expression for interface free energy and an adsorption equation for solid-fluid interface in binary system we first analyze conditions of thermodynamic equilibrium. Consider a rectangular block of material containing two coexisting binary phases, solid and fluid, separated by a planar interface. We assume that the solid phase is formed by the substitutional mechanism and is in a non-hydrostatic state of stress. The z direction of the block is perpendicular to the plane of interface. Boundary conditions in the x and y directions of the block are periodic.

Equilibrium conditions between multicomponent solid and fluid were derived by Larche and Cahn [13, 14]

- *Thermal equilibrium*: temperature T is uniform over the system.
- *Mechanical equilibrium:* Principal value of stress in the solid perpendicular to the solid-fluid interface is equal to minus pressure in the fluid $\sigma_{33} = -P$.
- *Chemical equilibrium:* diffusion potential M_{12} is uniform throughout the system. It is defined as a change in energy due to change in chemical composition of a

system when all other variables are held constant:

$$M_{21} \equiv \left(\frac{\partial U}{\partial N_2}\right)_{N,S,V,e_{ij}} \tag{10}$$

is constant everywhere in the system. Here, U , S, and V are the internal energy, entropy and volume of a region containing $N = N_1 + N_2$ atoms, where N_1 and N_2 are the numbers of atoms of species 1 and 2.

- *Phase-change equilibrium*: The following relation hold for homogeneous solid region

$$0 = U^s - TS^s + PV - \mu_1 N_1^s - \mu_2 N_2^s, \tag{11}$$

For a homohenious fluid region:

$$0 = U^f - TS^f + PV - \mu_1 N_1^f - \mu_2 N_2^f, \tag{12}$$

In Eqs. (11) and (12) superscripts s and f refer to the solid and fluid, respectively. μ_1 and μ_2 are chemical potentials of component 1 and 2 in the fluid. The diffusion potential is related to the chemical potentials via

$$M_{21} = \mu_2 - \mu_1 \tag{13}$$

By considering a virtual process of creation of interface we derived the following expression for interface free energy [39]

$$\gamma A = U - TS + PV - \mu_1 N_1 - \mu_2 N_2. \tag{14}$$

Solving the system of Eqs. (11), (12) and (14) we obtain an expression for γA in terms of excesses of extensive properties [11, 39]

$$\gamma A = [U]_{XY} - T[S]_{XY} + P[V]_{XY} - \mu_1[N]_{XY} - M_{21}[N_2]_{XY} \tag{15}$$

where X and Y are any two of the extensive properties S, V, N and N_2. The coefficients $[Z]_{XY}$ are defined through the following determinants [11]

$$[Z]_{XY} \equiv \frac{\begin{vmatrix} Z & X & Y \\ Z^s & X^s & Y^s \\ Z^f & X^f & Y^f \end{vmatrix}}{\begin{vmatrix} X^s & Y^s \\ X^f & Y^f \end{vmatrix}}. \tag{16}$$

The quantities in the first raw are computed for an arbitrary chosen region containing interface. The boundaries of this region are placed in the homogeneous phases. The quantities in the second and third raws are computed for arbitrary chosen regions inside homogeneous solid and fluid phases respectively. $[Z]_{XY}$ has a meaning of excess of quantity Z when the region containing interface has the same amounts of quantities

X and Y as homogeneous phases together. Since $[X]_{XY} = [Y]_{XY} = 0$, two terms in Eq. (15) can be eliminated by specifying X and Y. As a result, depending on the choice of X and Y γA can be expressed as an excess of different potentials. For example,

$$\gamma A = [U - TS + PV]_{NN_2} = [U - \mu_1 N - M_{12} N_2]_{SV} = [U - TS - \mu_1 N]_{VN_2} = ... \quad (17)$$

The following Gibbs-Duhem type equations can be derived for arbitrary chosen interface region and homogeneous solid and fluid regions [1, 39]

$$d(\gamma A) = -SdT + VdP - N_1 d\mu_1 - N_2 d\mu_2 + \sum_{i,j=1,2} (\sigma_{ij} + \delta_{ij} P) V de_{ij}, \quad (18)$$

$$0 = -S^s dT + V^s dP - N_1^s d\mu_1 - N_2^s d\mu_2 + \sum_{i,j=1,2} \left(\sigma_{ij}^s + \delta_{ij} P\right) V^s de_{ij}, \quad (19)$$

$$0 = -S^f dT + V^f dP - N_1^f d\mu_1 - N_2^f d\mu_2. \quad (20)$$

By solving the system of these three equations in conjunction with $M_{21} = \mu_2 - \mu_1$ and $N = N_1 + N_2$, we derive the adsorption equation [39]

$$d(\gamma A) = -[S]_{XY} dT + [V]_{XY} dP - [N]_{XY} d\mu_1 - [N_2]_{XY} dM_{21} + \sum_{i,j=1,2} [(\sigma_{ij} + \delta_{ij} P)V]_{XY} de_{ij}. \quad (21)$$

Here, X and Y are any two of the seven extensive properties S, V, N_1, N_2 and $(\sigma_{ij} + \delta_{ij} P)V$. Each differential coefficient $[Z]_{XY}$ is defined through determinants according to Eq. (16). Two terms in Eq. (21) can be eliminated by specifying X and Y leaving five independent variables.

The last term in Eq. (21) describes variations of γA due to elastic straining of the interface. Thus, Eq. (21) defines interface stress tensor τ_{ij} as a partial derivative of γA with respect to strain e_{ij} per unit area while all other independent variables are held constant:

$$\tau_{ij} = \frac{1}{A}\left(\frac{\partial(\gamma A)}{\partial e_{ij}}\right) = \frac{1}{A}[(\sigma_{ij} + \delta_{ij} P)V]_{XY} = \frac{1}{A}\frac{\begin{vmatrix} (\sigma_{ij} + \delta_{ij} P) V & X & Y \\ \left(\sigma_{ij}^s + \delta_{ij} P\right) V^s & X^s & Y^s \\ 0 & X^f & Y^f \end{vmatrix}}{\begin{vmatrix} X^s & Y^s \\ X^f & Y^f \end{vmatrix}}. \quad (22)$$

This equation represents the interface stress as an excess over bulk stresses and gives a recipe for its calculation for a general case of non-hydrostatic solids. Because τ_{ij} depends on the choice of X and Y, it is generally not unique.

Eliminating $[S]_{XY}$ from Eq. (21) by means of Eq. (15) we derive the Gibbs-Helmholtz type equation suitable for thermodynamic integration.

$$d\left(\frac{\gamma A}{T}\right) = -\frac{[\Psi]_{XY}}{T^2}dT + \frac{[V]_{XY}}{T}dP - \frac{[N]_{XY}}{T}d\mu_1 - \frac{[N_2]_{XY}}{T}dM_{12} + \frac{1}{T}\sum_{i,j=1,2}[(\sigma_{ij}+\delta_{ij}P)V]_{XY}\,de_{ij}, \tag{23}$$

where we denote

$$\Psi \equiv U + pV - \mu_1 N - M_{12}N_2. \tag{24}$$

Two variables can be eliminated from Eq. (23) by specifying X and Y. The resulting equation can be then integrated along any path on the phase coexistence surface to compute γ as a function of intensive variables.

For example, if we choose N and V for X and Y, then Eq. (23) becomes

$$d\left(\frac{\gamma A}{T}\right) = -\frac{[U - N_2M_{21}]_{NV}}{T^2}dT - \frac{[N_2]_{NV}}{T}dM_{12} + \frac{1}{T}\sum_{i,j=1,2}[(\sigma_{ij}+\delta_{ij}P)V]_{NV}\,de_{ij}. \tag{25}$$

We can also take N and N_2 for X and Y, which gives

$$d\left(\frac{\gamma A}{T}\right) = -\frac{[U+PV]_{NN_2}}{T^2}dT + \frac{1}{T}[V]_{NN_2}dP + \frac{1}{T}\sum_{i,j=1,2}[(\sigma_{ij}+\delta_{ij}P)V]_{NN_2}\,de_{ij}. \tag{26}$$

We can apply Eq. (25) and Eq. (26) to a process when pressure in the fluid is zero and constant , while T, M_{12} and e_{ij} vary. On this trajectory M_{21} and and e_{ij} are functions of T. This functional dependence can be described by

$$dM_{21} = \left(\frac{dM_{21}}{dT}\right)_{P,coex.}dT,$$

$$de_{ij} = \left(\frac{de_{ij}}{dT}\right)_{P,coex.}dT,$$

where the subscript $P, coex.$ indicates that the derivatives are taken on the phase coexistence surface at a constant pressure. Eqs. (25) and (26) can now be integrated along this path to give

$$\begin{aligned}\gamma A &= \frac{(\gamma A)_0\,T}{T_0} - T\int_{T_0}^{T}\Big(\frac{[U-N_2M_{21}]_{NV}}{T'^2} - \sum_{i,j=1,2}\frac{[(\sigma_{ij}+\delta_{ij}P)V]_{NV}}{T'}\left(\frac{de_{ij}}{dT}\right)_{P,coex.} + \\ &\quad + \frac{[N_2]_{NV}}{T'}\left(\frac{dM_{21}}{dT}\right)_{P,coex.}\Big)dT',\end{aligned} \tag{27}$$

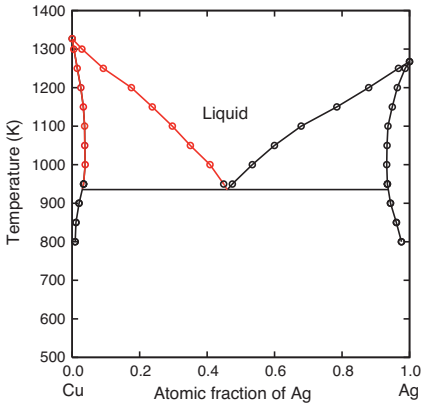

Figure 4: The Cu–Ag phase diagram predicted by the embedded-atom potential [40].

$$\gamma A = \frac{(\gamma A)_0 T}{T_0} - T \int_{T_0}^{T} \left(\frac{[U+PV]_{NN_2}}{T'^2} - \sum_{i,j=1,2} \frac{[(\sigma_{ij}+\delta_{ij}P)V]_{NN_2}}{T'} \left(\frac{de_{ij}}{dT} \right)_{P,coex.} \right) dT', \tag{28}$$

where superscript 0 refers to the initial state of the path.

Integration in Eqs. (27) and (28) are performed along the same path which corresponds to the same physical process and only differ in the choice of the properties X and Y selected to compute the excess quantities.

Thermodynamic relations derived for solid-fluid equilibrium in binary systems were applied to atomistic of simulations of (110) solid-liquid interface in CuAg alloy. The interactions between atoms were described by the EAM potential developed in Ref. [40]. This potential utilizes existing Cu [26] and Ag [40] potentials, with the cross-interaction function fit to first-principles formation energies of several imaginary compounds of the Cu-Ag system. This potential reproduces the Cu-Ag phase diagram (Fig. 4) in semi-quantitative agreement with experiment [41]. The melting point of Cu and the eutectic temperature predicted by this potential are 1327 K and 935 K, the experimental values being 1356 K and 1053 K, respectively [41]. The Cu-rich and Ag-rich solid solutions form by the substitutional mechanism.

The chemical compositions of the coexisting solid and liquid phases at different temperatures are defined by the solidus and liquidus lines shown in Figure 4 in red. As temperature decreases, starting from pure Cu, the concentration (atomic fraction) of Ag atoms in the liquid phase increases from 0 to 0.46 (eutectic composition), while the concentration in the solid phase never exceeds a few percent. This leads to very large composition differences across the interface at low temperatures.

The (110) orientation of the solid-liquid interface was chosen for this study because the same orientation was used in our previous work on pure Cu [25]. This interface was modeled in a rectangular $26 \times 25 \times 190$ Å (8,960 atoms) simulation block containing an 80 Å thick solid layer and two 55 Å thick liquid layers exposed to vacuum (Fig. 5).

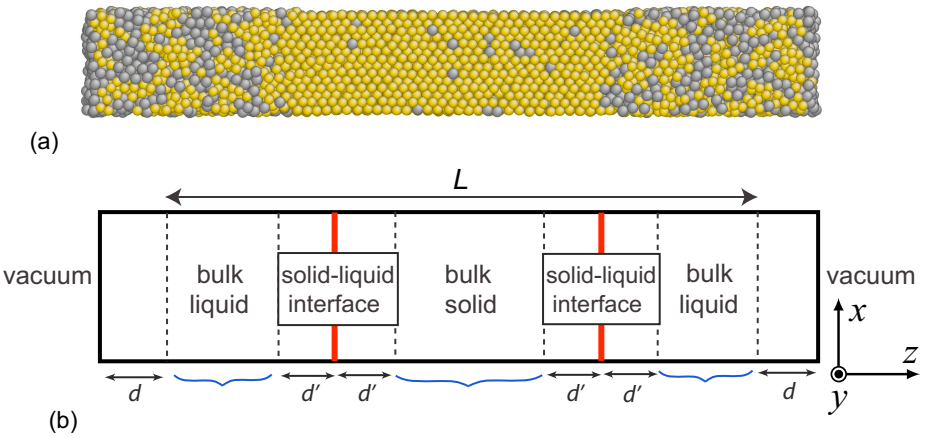

Figure 5: (a) Snapshot of the simulation block at 1000 K. The solid phase is sandwiched between two liquid layers, each exposed to vacuum to ensure zero pressure in the z-direction. The yellow and gray colors designate Cu and Ag atoms, respectively. (b) Schematic presentation of different regions involved in the calculations of excess quantities. L is the total thickness of the layer used for interface excess calculations. The solid-liquid interfaces are indicated by vertical red lines. The curly braces mark homogeneous solid and liquid regions.

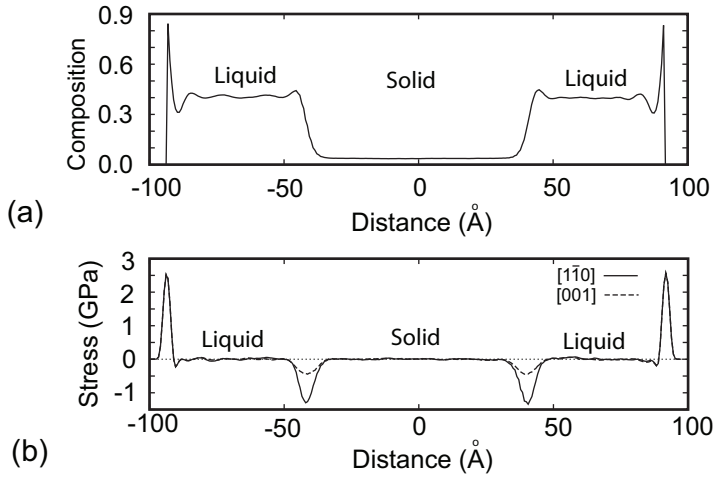

Figure 6: Profiles of a) Ag concentration and b) lateral components of stress at 1000K.

The $[1\bar{1}0]$ and [001] crystallographic directions of the solid part were aligned parallel to the x and y coordinate axes, respectively. Periodic boundary conditions were applied in the x and y directions, with free surfaces in the z direction. The exposure to vacuum guaranteed zero pressure in the liquid phase.

For each Monte Carlo (MC) simulation at a given value of diffusion potential and temperature, the simulation block was uniformly expanded by the thermal expansion factor corresponding to the simulated temperature and equilibrium chemical composition of the solid. The expansion factors were computed in separate MC simulations using a single-phase solid block. This pre-expansion procedure eliminated most of the thermal stresses that would otherwise be created in the solid phase. Nevertheless, some non-hydrostatic residual stresses remained due to statistical errors in the expansion factor. We, therefore, applied the full non-hydrostatic treatment of the problem to introduce corrections for the residual stresses.

The semi-grand canonical MC method [22, 42, 43] was applied to calculate equilibrium thermodynamic properties of the interface. In this method, the temperature, volume, total number of atoms N and the chemical potential difference M_{21} are held fixed, whereas positions and chemical sorts of atoms can vary. Each step of the MC process includes a random selection of an atom and its random displacement with a simultaneous random change of its chemical species. This trial move is accepted or rejected according to the Metropolis algorithm. Using this method, the equilibrium state of a binary system can be reached much faster than by molecular dynamics simulations, since the redistribution of chemical species in the MC method does not involve their actual diffusion (a very slow process in solids).

The MC simulations were performed at temperatures from $1327\,K$ (melting point of pure Cu) down to $1000\,K$. The values of M_{21} corresponding to solid-liquid coexistence at different temperatures were previously computed using the same MC technique [40]. For each T and M_{21}, the initial configuration of the simulation block was equilibrated

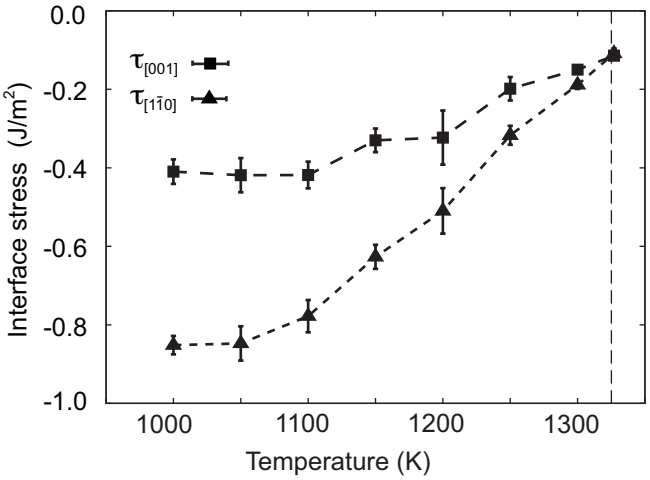

Figure 7: Principal components of the solid-liquid interface stress as functions of temperature. The vertical dashed line indicates the melting point of pure copper.

by 10^5 MC steps per atom, followed by a production run of 10^6 additional MC steps. Snapshot files containing instantaneous atomic positions, stresses and energies were saved every 50 MC steps and used for calculations of excess quantities at the post-processing stage. The stresses were computed from the standard virial expression.

Figure 6 illustrates profiles of composition and components of lateral stress. Concentration of silver in the bulk solid and liquid phases is very different. The stresses fluctuate around zero in the liquid phase and are very close to zero in the solid phase (residual thermal stresses are present due to mismatch in thermal expansion). The large concentration peaks at the ends of the composition profile reflect the strong segregation of Ag to the open surfaces of the liquid. Note that these peaks are followed by oscillations penetrating deep into the liquid. The large positive peaks of the lateral stress are due to the large positive tension of the open surfaces. Both stress components produce identical peaks, as expected from the anisotropy of the liquid surface.

The solid-liquid interfaces are characterized by smaller peaks of Ag concentration, whose positive sign is indicative of Ag attraction to these interfaces. The negative sign of the stress peaks suggests that the solid-liquid interface is under compression. The different magnitudes of the peaks for different stress components indicate that the interface stress is significantly anisotropic. It is interesting to note that the positions of the composition and stress peaks at the solid-liquid interfaces do not coincide, with the composition peaks being slightly shifted towards the liquid phase. At high temperatures, the Ag concentration peaks at the solid-liquid interfaces could not be resolved due to larger thermal fluctuations and more extensive interface movements.

The temperature dependence of the principal components of τ_{ij} is shown in Figure 7. In pure Cu, both components are negative and nearly equal. In the binary system they remain negative and their magnitude drastically increases with alloying. As T approaches the eutectic temperature, the average magnitude of the interface stress

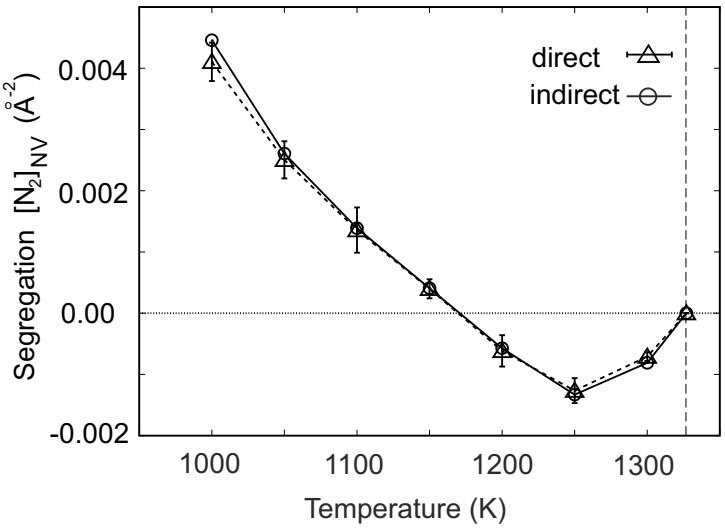

Figure 8: Ag segregation $[N_2]_{NV}$ at the solid-liquid interface as a function of temperature. The vertical dashed line indicates the melting point of pure copper.

becomes almost an order of magnitude larger than in pure Cu. Furthermore, the interface stress becomes highly anisotropic, with the magnitude of compression in the $[1\bar{1}0]$ direction being more than a factor of two larger than in the [001] direction.

The interface segregation $[N_2]_{NV}$ was calculated by two methods: directly using the determinants and indirectly using expression [39]

$$[N_2]_{NV} = \frac{[U]_{NN_2} - [U]_{NV}}{T\left(\dfrac{dM_{21}}{dT}\right)_{P,coex.}} - M_{21}. \tag{29}$$

The obtained temperature dependence of the segregation is plotted in Fig. 8. The good agreement between the direct and indirect calculations confirms the correctness of our methodology. Note that the segregation is negative at high temperatures but becomes positive below $1175K$. The temperature dependence of the segregation is almost linear when approaching the eutectic point.

Finally, Figure 9 displays the interface free energy obtained by thermodynamic integration (Eqs. (27) and (28)) as a function of T for different choices of X and Y. As expected, the results are identical within the accuracy of the calculations. γ *decreases* with decreasing temperature approximately linearly from $0.199\ J/m^2$ for pure copper to $0.178\ J/m^2$ in the alloy system at $1000\,K$. A similar trend was found in recent CFM calculations for a Lennard-Jones system with lens-type solid-liquid phase digram [37]. The variation of γ is much smaller than the change in the interface stress in the same temperature interval.

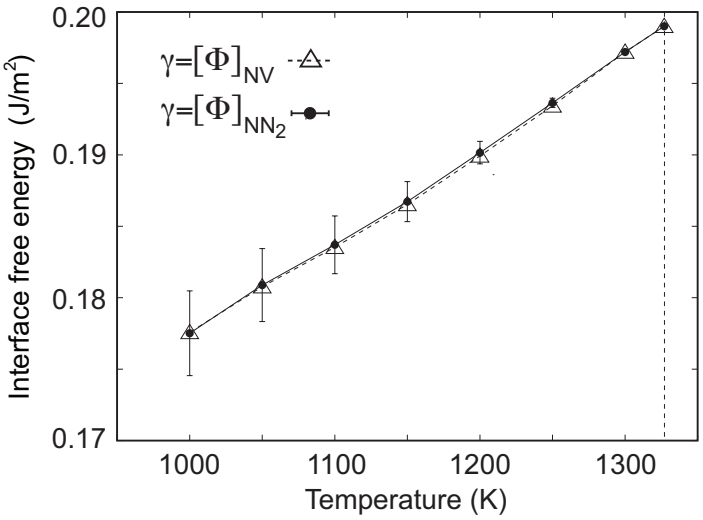

Figure 9: Temperature dependence of the solid-liquid interface free energy in CuAg alloy computed with different choices of the conserved properties X and Y. As expected, the computed values are identical within the accuracy of calculations. The vertical dashed line indicates the melting point of pure Cu.

4.3 Stable nanocolloidal structures in metallic systems

Gibbs showed that stability of fluid-fluid interfaces requires that interface tension γ be positive [1]. It is assumed that if γ was negative interface area would increase until phases completely mix. There is growing evidence, however, suggesting that on the sub-micrometer and especially nano-meter scales and in presence of surface-active agents, some interfaces can attain a negative tension and give rise to metastable or even stable disperse structures. For example, most of the liquid-liquid colloids (emulsions), such as oil in water, are thermodynamically unstable and tend to coarsen with time [44, 45]. However, some are believed to become thermodynamically stable in the presence of strong surfactants that drastically reduce γ or even make it negative [44, 46, 47]. A negative surface tension was found in recent relaxation dynamics experiments during vesicle deflation [48]. For solid-fluid surfaces, it has recently been found that dissociated water adsorbed on alumina surfaces can reduce γ to negative values, promoting the formation of a nano-porous material [49]. As another example, nano-size sheets of ZnS are found to be favored over bulk ZnS when processed in appropriate chemical environments [50]. Evidence of a negative surface tension stabilizing elongated cavities is reported in recent experimental studies of selective electrodissolution of β-brass [51]. Many important questions arise, such as why despite the negative γ the material reaches an equilibrium degree of dispersion instead of continuing to increase the interfacial area? Attempts to answer these questions through atomic-level modeling are hindered by the complex chemistry of the systems exhibiting negative γ.

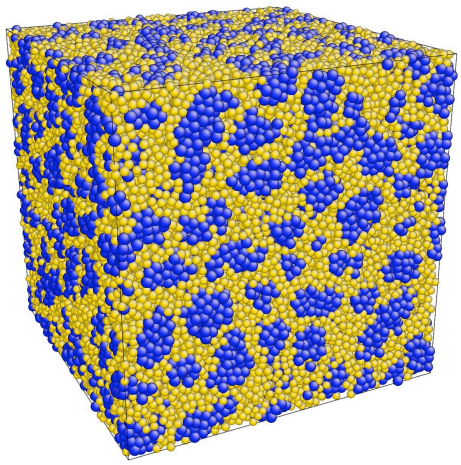

Figure 10: Equilibrium atomic structure of the Cu-Ta nano-colloid after a 30 ns MD simulation run at 2500 K. Ta nano-particles (blue) are suspended in liquid Cu (yellow). The initial state was a homogeneous liquid with a random distribution the species. The $11 \times 11 \times 11$ nm^3 simulation block has the average chemical composition of 33 $at.\%$Ta.

We performed a study of binary CuTa liquid modeled with semi-empirical potential that displays a stable nano-colloidal structure with Ta clusters embedded in Cu rich liquid. This system represent a simple model that exhibits negative interface tension and can be used to study stable nano-colloidal systems.

The interactions between Cu and Ta particles were modeled by angular-dependent many-body interatomic potential which was fit to experimental data and first-principles calculations [52]. The potential correctly predicts practically zero mutual solubility between solid Ta [53] and Cu [26]. The potential utilizes previously developed potentials for pure copper and tantalum. The melting points of pure Cu and Ta are $T_m = 1327K$ and $T_m = 3960K$ respectively. The phase diagram predicted by this potential is in qualitative agreement with the experimental one [41]. The diagram contains a liquidus line connecting T_m's of pure Cu and Ta, a eutectic point which practicaly coincides with T_m of Cu, and a metastable liquid-liquid miscibility gap.

To model CuTa liquid system we used simulation block with periodic boundary conditions with dimensions $11 \times 11 \times 11$ nm^3. Simulations were performed in NPT ensemble with Nose-Hoover thermostat. Simulations with 33% Ta concentration were performed at $2500K$, $2750K$ and $3000K$. Simulations at $2500K$ were also performed for 20% and 25% of Ta.

We found that initially homogeneous solutions of Cu and Ta would quickly transforms into colloidal structure illustrated of Figure 10. The Ta particles are embeded in Cu rich liquid and have a nearly spherical shape. The amount of Ta in the Cu matrix is on the order of 1%. The Ta particles are uniformly distributed in the simulation block.

We implemented an automatic procedure of identification of individual Ta particles.

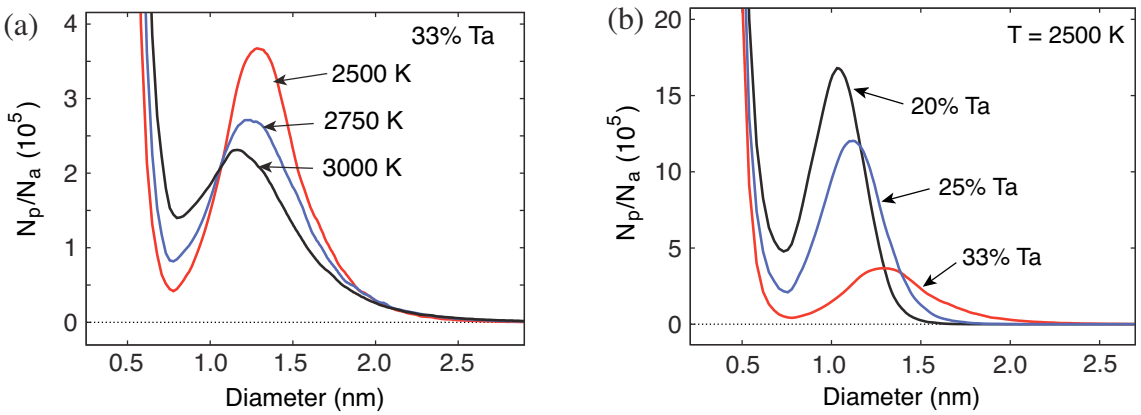

Figure 11: Distribution of effective particle diameters in Cu-Ta colloids (a) at three different temperatures for the same average chemical composition of 33 at.%Ta, and (b) at three different chemical compositions for the same temperature of 2500 K. The vertical axis gives the number of particles N_p with a given diameter relative to the total number of atoms $N_a \approx 10^5$. The peak represents the most typical particles forming the colloid. The sharp increase at small sizes is caused by individual Ta atoms and small dynamic clusters (short-range order) in liquid Cu, which are also identified by our algorithm as "particles".

The algorithm selects a random Ta atom and then performs a random walk within neighbors of each selected atom until all atoms belonging to one particle are identified. Nearest neighbors are identified using a search radius slightly large then the position of the first peak in the Ta-Ta pair distribution function, $R_1 = 0.28nm$. The algorithm calculates the number of Ta atoms in a particle. The effective diameter of a particle was related to number of atoms via relation $D = 1.24(n\Omega)^{1/3}$, where the numerical coefficient assumes the spherical shape of the particle and Ω is atomic volume of liquid Ta. Figure 11 demonstrates size distribution of Ta particles for simulated temperatures and compositions.The relatively sharp peak in size distribution corresponds to the typical particle size of around 1 to 1.5 nm ($n \approx 30 - 60$ atoms). The part of the distribution function near the origin corresponds to individual atoms in the Cu matrix identified as particles by the algorithm. The tail of the distribution function corresponds to collisions of particles. The average size of the particles increases with composition at a given temperature and decreases with temperature for a fixed composition.

The atomic motion in the colloid was examined by tracing the motion of groups of labeled atoms. During the simulations ($30ns$) atoms of Cu and Ta diffuse over distances exceeding the size of the simulations block, which shows that the system had enough time to coarse structure if the latter was thermodynamically favorable. However, we did not observe processes of coarsening. Ta particles move by Brownian motion. They occasionally collide with one another, sometime briefly merge and then break apart, while constantly exchanging atoms by diffusion through liquid Cu.

To check that the colloidal structure is stable against coarsening we introduced a

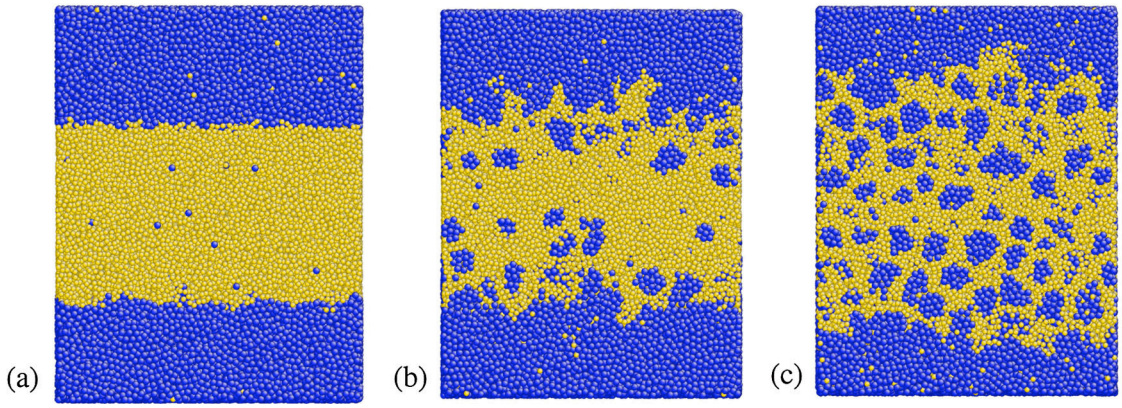

Figure 12: Interaction of Cu (yellow) and Ta (blue) liquids during MD simulations at 2500 K. (a) after 20 ps; the liquid-liquid interfaces are relatively sharp, (b) after 680 ps; the interfaces is already rugged and Ta atoms diffusing into Cu begin to from colloidal particles, (c) after 2 ns; a nano-colloid has formed between the Ta liquid layers. The average chemical composition of the $12 \times 16 \times 9$ nm^3 simulation block is 50 at.%Ta.

Ta particle five times the size the typical particle. To do so we switched atomic sorts of Cu atoms to Ta. Within 100 ps of the subsequent simulation the particle would break into smaller ones. As another test of stability we created a simulation block that contained Ta rich and Cu rich liquids initially separated by a plane interface. During the subsequent simulation the initial structure quickly changes as illustrated on Figure 12. Within first 40 ps interface becomes extremely rugged with Ta particles chipping away into the liquid Cu. The simulation showed that the plane interface is unstable with respect to transformation into colloidal structure.

To explain the observed structure we proposed a simple phenomenological model. The model predicts that even if interface tension is negative the structure can be stable if γ is curvature dependent. We assume that γ can be expanded in powers of curvature k [54, 55]

$$\gamma(k) = \gamma_0 + ak + bk^2 + ck^3 + ... \tag{30}$$

The contribution to free energy from interfaces is then

$$G(k) = \frac{A_1}{k_1}\left(\gamma_0 k + ak^2 + bk^3 + ck^4 + ...\right) \tag{31}$$

Possible behaviors of γ and G are illustrated in Figure 13. Three different cases are possible with G attaining minimum required to stabilize th e structure. In case I and II γ_0 is positive. In case I the colloid is metastable with respect to plane interface, whereas in case II the colloid is more stable. In case III , γ_0 is negative and G reaches two negative minima. Thus two stable colloids are possible. These calloids are inverse to each other. Our simulations are compatible with cases II and III.

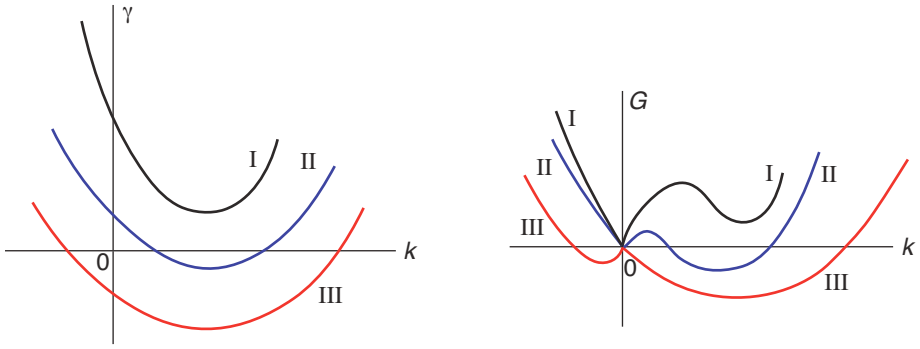

Figure 13: Schematic presentation of the interface tension γ and the total interface free energy G as functions of curvature k for a set of spherical particles at a constant total volume. All three cases give a minimum of G stabilizing the particles with a finite size (colloidal state). In case I the colloid is metastable relative to a plane interface ($k \to 0$), which is the stable state of the system. In case II the colloid is more stable than the plane interface but the latter remains metastable. In case III two stable colloidal states are possible while the plane interface is unstable.

The system studied is fundamentally different from traditional colloids. The negative tension is not caused by surfactants but represents an intrinsic property of the system. Such systems represent an intriguing and poorly understood state of condensed matter, which deserves attention. Interfaces with a negative tension may exist in very diverse physical systems, ranging from emulsions to biological cells (vesicles) [48], to superconductor-normal interfaces showing negative γ values (type-II superconductors) [56].The potential for Cu-Ta system provides a simple model to study systems with negative tension. These systems represent a new and state of condensed matter.

5 Future work

5.1 Non-hydrostatic solid-liquid equilibrium in a single component system

In Refs. [57, 39] we analized thermodynamics of solid-fluid interfaces for a general case of non-hydrostatic equilibrium. We derived equations that allow to compute interface free energy and interface stress along an equilibrium trajectory in configuration space. However, so far we only applied the treatment to nearly hydrostatic systems. In the following two sections we discuss how a trajectory of non-hydrostatic solid-liquid equilibrium for a single component system can be computed in atomistic simulations and how interface properties can be computed along this trajectory.

5.1.1 Bulk equilibrium

Equilibrium between non-hydrostatically stressed solid and fluid was first discussed by Gibbs [1]. He derived the following equilibrium conditions: 1) temperature T is uniform throughout the system 2) Principal axis of the stress σ_{33} in the solid is perpendicular to the solid-fluid interface and $\sigma_{33} = -P$, where P is pressure in the fluid, 3) the following relation holds

$$u^s - Ts^s + P\Omega^s = \mu \tag{32}$$

where u^s, s^s and Ω^s are energy, entropy and volume per atom in the solid and μ is the chemical potential in the fluid.

Gibbs pointed out that fluid equilibrated with solid is supersaturated with respect to substance of solid except when solid is hydrostatic. He pointed out that for variations away from hydrostatic state at a constant pressure P in the liquid the temperature change is zero to first order. Using isotropic linear elasticity, Sekerka and Cahn showed that for this process the change of equilibrium temperature is quadratic with respect to non-hydrostatic components of stress [58]. This means that if solid becomes non-hydrostatic while the change of the trace of the stress tensor is zero, the temperature will still decrease. Non-hydrostatic solid cannot be treated as hydrostatic by assigning to it pressure equal to average of principal stresses. Predictions of hydrostatic treatments (for example Claperon-Claysius trajectory) will not be valid.

The analysis of Sekerka and Cahn addresses only a particular process (constant P) while equilibrium conditions and Gibbs equation for variation of the state of the system at equilibrium were derived for a general case that includes variations of pressure. In this work we will analyze a general variation in the state of the non-hydrostatic system and use anisotropic linear elasticity to evaluate both temperature and pressure change as functions of non-hydrostatic stresses in the solid phase. The expressions for temperature and pressure change would involve thermodynamic quantities that can be easily computed in atomistic simulations.

We will check our theory using atomistic modeling. We will use copper as a model material with interactions in described by EAM potential [59]. To model solid-liquid equilibrium we will create a simulation block containing solid phase sandwiched between two liquid layers with (110) interface perpendicular to the z direction. Boundary conditions in the x and y directions will be periodic with the $[\bar{1}10]$ and [001] crystallographic directions of the solid phase parallel to the x and y directions respectively. No periodic boundary conditions will be applied in the z directions to create two liquid surfaces. Exposure of liquid phases to vacuum ensures zero pressure P in the bulk of the liquid phase. The structure should be then equilibrated during MD run in NVT ensemble at $T_m = 1327K$.

To obtain simulation blocks with solid phase under non-hydrostatic state of stress we will deform initial simulation block parallel to the solid-liquid interface. Due to the liquid surfaces, component of stress normal to the interface will remain zero. To sample different states of stress we will apply four types of deformation: biaxial compression,

biaxial tension, compression in the $[\bar{1}10]$ direction with simultaneous tension in the [001] direction and tension in the $[\bar{1}10]$ direction with simultaneous compression in the [001] direction.

Solid with non-hydrostatic stresses at T_m is not in equilibrium with its melt. Subsequent MD runs performed in NVT ensemble at T_m would result in a complete melting of the solid phase. To find the temperature at which non-hydrostatic solid is in equilibrium with liquid we need to performe simulations in the micro-canonical ensemble (NVE). In this ensemble the system is adiabatic and there is no supply of heat from the outside required to melt the solid phase. When solid phase partually melts (crystallizes) by thermal fluctuations, the absorbed (released) latent heat comes from (supplied to) the kinetic energy of atoms. This means that the temperature of the system changes, counteracting continuous melting (crystallization). As a result, the temperature of the system fluctuates around an equilibrium one.

To collect the data for subsequent analysis we will run a simulation in NVE ensemble (production stage). During the run snapshots of the system will be generated every $0.01\,ns$. The snapshots containe positions of the atoms, stresses and energies of individual atoms. Equilibrium temperature T_N for a given state of stress can be computed by averaging instantaneous temperatures during the production stage.

After we compute several equilibrium temperatures as a function of non-hydrostatic stresses we will be able to compare them with predictions of theory.

5.1.2 Interface thermodynamics

Knowing the non-hydrostatic solid-liquid coexistence surface in the configuration space we will study interface properties. For a single component system interface free energy can be expressed as an excess of the following potential [39]

$$\gamma A = [U - TS + PV - \mu N]_{XY} \tag{33}$$

where X and Y are two of the extensive properties S, V and N. Quantities $[Z]_{XY}$ are computed using determinants in Eq. (16). The adsorption equation is given by

$$d(\gamma A) = -[S]_{XY}\, dT + [V]_{XY}\, dP - [N]_{XY}\, d\mu + \sum_{i,j=1,2} [(\sigma_{ij} + \delta_{ij} p)V]_{XY}\, de_{ij} \tag{34}$$

X and Y are any of the extensive properties S, V, N or $(\sigma_{ij} + \delta_{ij}P)V$. By specifying X and Y two terms in Eq. (34) can be eliminated. The remaining variables will be independent. It is important to carefully analyze the number of degrees of freedom as well as sets of independent variables predicted by Eq. (34).

The last term in Eq. (34) has a meaning of change of γA due to elastic stretching and can be identified with interface stress tensor $\hat{\tau}$. The components of this second rank tensor are given by

$$\tau_{ij}^{XY} = \frac{1}{A}\frac{\partial\left(\gamma A\right)}{\partial e_{ij}} = \frac{1}{A}\left[(\sigma_{ij}+\delta_{ij}p)V\right]_{XY} = \frac{1}{A}\frac{\begin{vmatrix} (\sigma_{ij}+\delta_{ij}p)\,V & X & Y \\ \left(\sigma_{ij}^{s}+\delta_{ij}p\right)V^{s} & X^{s} & Y^{s} \\ 0 & X^{f} & Y^{f} \end{vmatrix}}{\begin{vmatrix} X^{s} & Y^{s} \\ X^{f} & Y^{f} \end{vmatrix}}. \quad (35)$$

Variables held constant in the variation in Eq. (35) depend on the choice of extensive quantities X and Y . As we pointed out earlier, $\hat{\tau}$ is not unique and depends on X and Y. The only exception is the hydrostatic case when $\sigma_{ij}^{s}+\delta_{ij}P = 0$ and $\tau_{ij} = (\sigma_{ij}+\delta_{ij}P)\,V/A$ is independent of X and Y.

As in the work on solid-liquid equilibrium in CuAg system, here we can choose $X = N$ and $Y = V$ and compute the interface stress along the non-hydrostatic equilibrium trajectory obtained by biaxial tension and biaxial compression.

Another possible choice for X and Y that can be directly computed from atomistic simulations is when one of the extensive variables is equal to one of the non-hydrostatic components of stress $(\sigma_{11}+P)V$ or $(\sigma_{22}+P)V$. We will compute these interface stresses along the non-hydrostatic equilibrium trajectory and compare with the previous interface stress. Using thermodynamic equations we can derive relations between different interface stresses and verify this relations by atomistic simulations.

Gibbs-Helmholtz type equation suitable for thermodynamic integration has form

$$d\left(\frac{\gamma A}{T}\right) = -\frac{[\Psi]_{XY}}{T^{2}}dT + \frac{[V]_{XY}}{T}dP - \frac{[N]_{XY}}{T}d\mu + \frac{1}{T}\sum_{i,j=1,2}\left[(\sigma_{ij}+\delta_{ij}P)V\right]_{XY}de_{ij}, \quad (36)$$

where $\Psi \equiv U + PV - \mu N$ and does not contain the entropy term. Eq. (36) can be integrated from some reference temperature T_0 to recover γ.

By performing thermodynamic integration from point of hydrostatic equilibrium we can compute γ for branches of biaxial compression and tension. Since the pressure in the liquid for this trajectory is constant and zero, choosing X=N, Y=V and integrating Eq. (36) we obtain

$$\gamma A = \frac{(\gamma A)_0\,T}{T_0} - T\int_{T_0}^{T}\left(\frac{[U]_{NV}}{T'^{2}} - \sum_{i,j=1,2}\frac{\left[(\sigma_{ij}+\delta_{ij}P)V\right]_{NV}}{T'}\left(\frac{de_{ij}}{dT}\right)_{P,coex.}\right)dT' \quad (37)$$

The derivative $(de_{ij}/dT)_{P,coex}$ is taken along the coexistence trajectory. Quantities in the integrand of Eq. (37) are readily accessible in atomistic calculations.

5.2 Thermodynamics of grain boundaries in multicomponent systems under applied mechanical stresses

5.2.1 Challenges in thermodynamic treatment of grain boundaries and our approach

Grain boundary (GB) is an interface between two solid grains with different crystallographic orientations of the same material. Thus, it is an interface in a single phase system. We already discussed the case of a single phase when we analyzed thermodynamics of surfaces. GB thermodynamics is different from surfaces because they can support stresses normal to GB plane (just as two phase systems) and shear stress parallel to the GB plane. Support of shear parallel to the plane of interface is specific to solid-solid coherent interfaces.

Normal and shear components of stress represent new state variables that have to be incorporated into the thermodynamic treatment of interfaces in single-phase systems. The first step in developing the theory is derivation of γA as a reversible work of creation of GB. We will proceed in a manner similar to Ref. [39] analyzing the case of multicomponent system with both substitutional and interstitional components. We will consider a virtual process of creation of GB out of a single crystal. The difference in energies of the system with a GB and the reference bulk system is due to the heat supplied, mechanical work of normal and shear stresses, chemical work of change of local composition in the GB region and reversible work of interface creation γA. Once the expression for GB free energy is derived we can use it to derive an adsorption equation and Gibbs-Helmholtz type equation for thermodynamic integration. These equations imply Maxwell type relations between second derivatives of γA (derivatives of excess properties).

5.2.2 Atomistic simulations of grain boundaries

We will then apply the theory to atomistic simulations. As a model material we will use pure copper and copper-silver alloy, with atomic interactions described by EAM potentials mentioned earlier [60, 40]. We will use a symmetrical tilt $\Sigma 5(310)$ GB as a model structure. The boundary is created from a single grain by a rotation of the upper half of the grain around [001] direction (tilt axes) by 37 degrees. The structure of the boundary is illustrated on Figure 14. Due to the symmetry properties, the equilibrium between the grains is preserved when shear is applied parallel to the tilt axis.

We will first test the theory for a single component at $0\,K$. The advantage of $0\,K$ calculations is that all the excesses including γ can be computed directly. Therefore, we can check our methodology by computing γ directly and by thermodynamic integration. We will apply four types of deformation: uniaxial lateral strain, biaxial lateral strain, tension/compression normal to the GB plain and shear parallel to the GB plain. For each type of deformation several deformed states will be created to sample a certain range of strain (or stress) variables. Each state will be relaxed and excess properties will be computed. Knowing the behavior of the excess quantities as functions of state

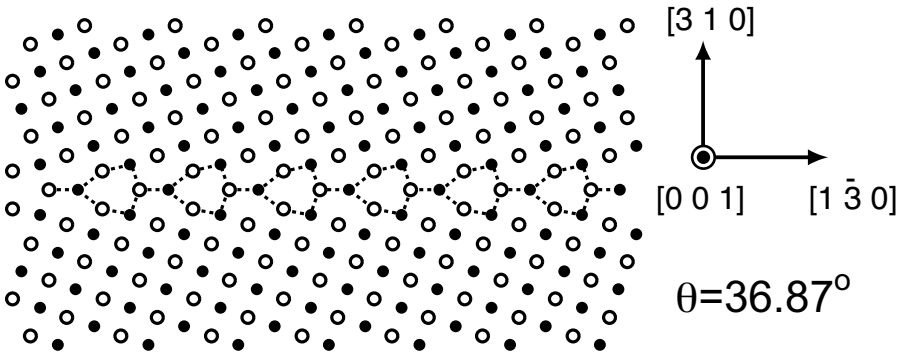

Figure 14: Atomic structure of [001] symmetrical tilt $\sum 5$ (310) ($\theta = 36.87^o$) GB in copper at 0 K. The filled and open circles represent rows of atoms with positions in alternating (0 0 2) planes. The structural units and the GB plane are outlined. The coordinate axes indicate crustallographic directions.

variables, we will be able to perform thermodynamic integration and check Maxwell relations.

Once the $0\,K$ case is analyzed, we will proceed by studying properties of the GB at finite temperatures. To model the bicrystall at different temperatures we will use MD simulations. The simulations will be performed in NVT ensemble with Nose-Hoover thermostat from $0\,K$ to $900\,K$ with $100\,K$ interval. At each temperature, the structure will be preexpanded according to the thermal expansion to minimize bulk stresses. The structures will be first equilibrated. The equilibration stage will be followed by a production stage during which snapshots of the system will be generated. These snapshots will be used later to compute excess properties required for thermodynamic integration. The reference value of γ can be computed at $300K$ using harmonic approximation [22]. GB free energy can be then recovered in the simulated temperature range by thermodynamic integration.

The next step is to compute GB excess properties in a binary CuAg system as a function of composition at a fixed finite temperature. To model GB alloy we will employ MC simulations in semi-grand canonical ensemble. In this ensemble atomic sorts are allowed to change at random with a probability determined by diffusion potential M_{12}, which is an input parameter of the simulations. By performing simulations with different values of M_{12} we can sample different chemical compositions. In this work we will model a copper-rich bicrystal.

To observe a sufficient amount of silver in the bulk copper we will perform simulations in the upper temperature range of the pure copper simulations. We will perform several MC simulations so that the bulk composition of silver changes from 0 (pure copper) to values close to the solubility limit at that temperature. At each simulation the block will be preexpanded according to the expansion for this temperature and bulk composition to minimize bulk stresses. Excess properties required for thermodynamic integration will then be computed as functions of the bulk composition. The reference

value of γ will be known from the thermodynamic integration for pure copper.

To verify Maxwell relations we will need to compute partial derivatives of excess quantities. To compute excess quantities as functions of intensive variables we select a state at finite temperature in binary system and perform four types of simulations: 1) biaxial deformation at constant T, M_{12}, σ_{33} and σ_{13}, 2) normal compression/tension at constant e_L, T, M_{12}, σ_{13} 3) change M_{12} at constant e_L, T, σ_{33} and $\sigma_{13}$and 4) change T at constant e_L, M_{12}, σ_{33} and σ_{13}. After we compute excess properties for all these variations, the derivatives can be evaluated for this particular state. These simulations will also demonstrate effects of mechanical deformation on segregation.

6 Publications and Presentations

6.1 Publications

- T. Frolov and Y. Mishin: Temperature dependence of the surface free energy and surface stress: An atomistic calculation for Cu(110), Physical Review B, 79, 045430, 2009
- T. Frolov and Y. Mishin: Molecular dynamics modeling of self-diffusion along a triple junction, Physical Review B, 79, 174110, 2009
- T. Frolov and Y. Mishin: Solid-liquid interface free energy in binary systems: Theory and atomistic calculations for the (110) Cu–Ag interface, The Journal Of Chemical Physics 131, 054702, 2009
- T. Frolov and Y. Mishin: Stable Nanocolloidal Structures in Metallic Systems, Physical Review Letters, 104, 055701, 2010
- T. Frolov and Y. Mishin: Orientation dependence of the solid-liquid interface stress: atomistic calculations for copper, submitted for publication in Modeling and Simulation in Material Science and Engineering
- T. Frolov and W. J. Boettinger and Y. Mishin: Atomistic simulation of hillock growth, submitted for publication in Acta Materialia

6.2 Presentations

T. Frolov and Y. Mishin: Temperature dependence of the surface free energy and surface stress: an atomistic calculation for (110) Cu, CMSN meeting, Princeton University, NJ, September 22, 2008.

T. Frolov and Y. Mishin: Solid-liquid interface free energy and interface stress in binary systems, CMSN meeting, San Francisco, CA, January 15, 2009.

T. Frolov and Y. Mishin: Atomistic modeling of interface thermodynamics (non-hydrostatic solids), TMS Annual meeting, San Francisco, CA, January 15, 2009.

T. Frolov and Y. Mishin: Molecular dynamic modeling of self diffusion along a triple junction, TMS Annual meeting, San Francisco, CA, January 15, 2009.

W. J. Boettinger, T. Frolov, and Y. Mishin: Stress-driven Surface Evolution during Whisker and Hillock Formation, TMS Annual meeting, San Francisco, CA, January 15, 2009.

T. Frolov and Y. Mishin: Thermodynamics of strongly non-hydrostatic solid-liquid interfaces: Theory and atomistic simulations, CMSN meeting, George Mason University, September 16, 2009.

T. Frolov and Y. Mishin: Thermodynamics of solid-fluid interfaces with non-hydrostatically stressed solids, TMS Annual meeting, Seattle, WA, 2010, Febrary 14-18, 2010.

T. Frolov and Y. Mishin: Effect of stresses on grain boundary thermodynamics: theory and atomistic simulations, TMS Annual meeting, Seattle, WA, 2010, Febrary 14-18, 2010.

T. Frolov, Y. Mishin, J. W. Cahn, Effect of pre-melting on grain boundary properties, TMS Annual meeting, Seattle, WA, 2010, Febrary 14-18, 2010.

T. Frolov, Y. Mishin: Atomistic Modeling of Solid-Liquid Interfaces Subject to Lateral Stresses, TMS Annual meeting, Seattle, WA, 2010, Febrary 14-18, 2010 (poster session).

References

[1] J. W. Gibbs, *The Scientific Papers of J. Willard Gibbs*, volume 1, Longmans-Green, London, 1906.

[2] A. P. Sutton and R. W. Balluffi, *Interfaces in Crystalline Materials*, Clarendon Press, Oxford, 1995.

[3] M. Asta et al., Acta Mater. **57**, 941 (2009).

[4] D. Herlach, P. Galenko, and D. Holland-Moritz, *Metastable Solids from Undercooled Melts*, Elsevier, Boston, MA, 2007.

[5] G. Ghosh, Mater Sci Eng A **189**, 277 (1994).

[6] T. Volkmann, W. Loeser, and D. N. Herlach, Metall Mater Trans A **28** (1997).

[7] D. M. Herlach, J Phys Condens Matter **13**, 7737 (2001).

[8] P. S. Ho and T. Kwok, Rep. Prog. Phys. **52**, 301 (1989).

[9] F. Mugele and J. Baret, J. Phys.: Condens. Matter **17**, 705 (2005).

[10] J. H. Song, R. Evans, Y.-Y. Lin, B.-N. Hsu, and R. B. Fair, Microfluid Nanofluid **7**, 75 (2009).

[11] J. W. Cahn, Thermodynamics of solid and fluid surfaces, in *Interface Segregation*, edited by W. C. Johnson and J. M. Blackely, chapter 1, page 3, American Society of Metals, Metals Park, OH, 1979.

[12] R. Shuttleworth, Proc. Phys. Soc. **63**, 444 (1949).

[13] F. Larche and J. W. Cahn, Acta Metall. **21**, 1051 (1973).

[14] F. C. Larche and J. W. Cahn, Acta Metall. **26**, 1579 (1978).

[15] M. S. Daw and M. I. Baskes, Phys. Rev. B **29**, 6443 (1984).

[16] D. Kramer and J. Weissmuller, Surf. Sci. **601**, 3042 (2007).

[17] J. W. M. Frenken, P. M. J. Maree, and J. F. van der Veen, Phys. Rev. B **34**, 7506 (1986).

[18] C. Gurney, Proc. Phys. Soc. **62**, 639 (1949).

[19] G. L. J. Bailey and H. Watkins, Proc. Phys. Soc. **63**, 350 (1949).

[20] C. Herring, The use of classical macroscopic concepts in surface-energy problems, in *Structure and Properties of Solid Surfaces*, edited by R. Gomer and C. S. Smith, chapter 1, pages 5–81, The Univ. of Chicago Press, Chicago, Illinois, 1953.

[21] J. S. Vermaak and D. K. Wilsdorf, J. Phys. Chem. **72**, 4150 (1968).

[22] S. M. Foiles, Phys. Rev. B **49**, 14930 (1994).

[23] J. Q. Broughton and G. H. Gilmer, Acta Metall. **31**, 845 (1983).

[24] C. A. Becker, D. L. Olmsted, M. Asta, J. J. Hoyt, and S. M. Foiles, Phys. Rev. Lett. **98**, 125701 (2007).

[25] T. Frolov and Y. Mishin, Phys. Rev. B **79**, 45430 (2009).

[26] Y. Mishin, M. J. Mehl, D. A. Papaconstantopoulos, A. F. Voter, and J. D. Kress, Phys. Rev. B **63**, 224106 (2001).

[27] L. E. Murr, *Interfacial Phenomena in Metals and Alloys*, Addison-Wesley, Reading, MA, 1975.

[28] R. C. Cammarata, Philos. Mag. **88**, 927 (2008).

[29] C. A. Becker, M. Asta, J. J. Hoyt, and S. M. Foiles, J. Chem. Phys. **124**, 164708 (2006).

[30] R. Sibug-Aga and B. B. Laird, J. Chem. Phys. **116**, 3410 (2002).

[31] R. Sibug-Aga and B. B. Laird, Phys. Rev. B **66**, 144106 (2002).

[32] H. Ramalingam, M. Asta, A. van de Walle, and J. J. Hoyt, Interface Sci. **10**, 149 (2002).

[33] J. Q. Broughton and G. H. Gilmer, J. Chem. Phys. **79**, 5095 (1983).

[34] R. L. Davidchack and B. B. Laird, Phys. Rev. Lett. **85**, 4751 (2000).

[35] J. J. Hoyt, M. Asta, and A. Karma, Phys. Rev. Lett. **86**, 5530 (2001).

[36] M. Amini and B. B. Laird, Phys. Rev. B **78**, 144112 (2008).

[37] C. A. Becker, D. L. Olmsted, M. Asta, J. J. Hoyt, and S. M. Foiles, Phys. Rev. B **79**, 054109 (2009).

[38] M. Asta, J. J. Hoyt, and A. Karma, Phys. Rev. B **66**, R100101 (2002).

[39] T. Frolov and Y. Mishin, J. Chem. Phys. **131**, 054702 (2009).

[40] P. L. Williams, Y. Mishin, and J. C. Hamilton, Modelling Simul. Mater. Sci. Eng. **14**, 817 (2006).

[41] T. B. Massalski, editor, *Binary Alloy Phase Diagrams*, ASM, Materials Park, OH, 1986.

[42] S. M. Foiles, Phys. Rev. B **32**, 7685 (1985).

[43] D. Frenkel and B. Smit, *Understanding molecular simulation: from algorithms to applications*, Academic, San Diego, second edition, 2002.

[44] P. Becher, *Emulsions. Theory and Practiice*, Oxford University Press, Oxford, New York, 2001.

[45] T. G. Mason, J. N. Wilking, K. Meleson, C. B. Chang, and S. M. Graves, J. Phys.: Condens. Matter **18**, R635 (2006).

[46] E. Ruckenstein, Advances in Colloid and Interface Science **79**, 59 (1999).

[47] J. T. G. Overbeek, Faraday Discuss. Chem. Soc. **65**, 7 (1978).

[48] V. Kantler, E. Serge, and V. Steinberg, Phys. Rev. Lett. **99**, 178102 (2007).

[49] Z. Lodziana, N. Y. Topsoe, and J. K. Nørskov, Nature Mater. **3**, 289 (2004).

[50] Z. Lin, B. Gilbert, Q. Liu, G. Ren, and F. Huang, J. Am. Chem. Soc. **128**, 6126 (2006).

[51] H. Martin, P. Carro, A. H. Creuz, R. C. Salvarezza, and A. J. Arvia, Phys. Rev. B **58**, 9666 (1998).

[52] A. Hashibon, A. Y. Lozovoi, Y. Mishin, C. Elsässer, and P. Gumbsch, Phys. Rev. B **77**, 094131 (2008).

[53] Y. Mishin and A. Y. Lozovoi, Acta Mater. **54**, 5013 (2006).

[54] H. P. Aubauer, J. Phys. F: Met. Phys. **8**, 375 (1978).

[55] R. C. Tolman, J. Chem. Phys. **17**, 333 (1949).

[56] H. Frahm, S. Ullah, and A. T. Dorsey, Phys. Rev. Lett. **66**, 3067 (1991).

[57] T. Frolov and Y. Mishin, Phys. Rev. B **79**, 045430 (2009).

[58] R. Sekerka and J. Cahn, Acta Mater. **52**, 1663 (2004).

[59] Y. Mishin, M. J. Mehl, and D. A. Papaconstantopoulos, Acta Mater. **53**, 4029 (2005).

[60] Y. Mishin, D. Farkas, M. J. Mehl, and D. A. Papaconstantopoulos, Phys. Rev. B **59**, 3393 (1999).